ACS APPLIED MATERIALS & INTERFACES

Letter

www.acsami.org

Hydrogen-Bonding-Facilitated Layer-by-Layer Growth of Ultrathin Organic Semiconducting Films

Sang-Mi Jeong, Taek-Gyoung Kim, Eunyoung Jung, and Ji-Woong Park*

School of Materials Science and Engineering, Gwangju Institute of Science and Technology, 261 Cheomdan-gwagiro, Buk-Gu, Gwangju 500-712, Korea

Supporting Information

ABSTRACT: We demonstrated that the layer-by-layer growth of thin film crystals of conjugated organic molecules is facilitated by their hydrogen-bonding capabilities. We synthesized bis(3-hydroxypropyl)-sexithiophene (bHP6T), which includes two hydroxyalkyl groups that promote interlayer and intermolecular molecular interactions during the crystal growth process. Under the optimal deposition conditions, the crystals grew in a nearly perfect layer-by-layer mode on the solid substrate surfaces, enabling the formation of uniform charge transporting films as thin as a few monolayers. A thin film transistor device prepared from a bHP6T film only 9 nm thick exhibited a charge carrier mobility well above 1×10^{-2} $cm^2/(V\ s)$ and an on/off ratio exceeding 1×10^4. These properties are better than the properties of other sexithiophene-based devices yet reported. The devices exhibited enhanced stability under atmospheric conditions, and they functioned properly, even after storage for more than 2 months.

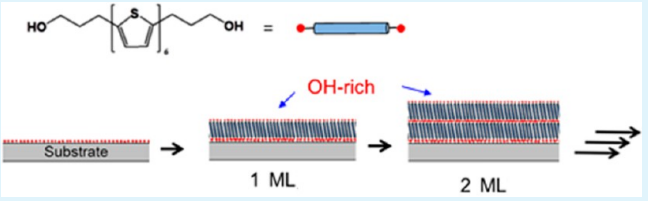

KEYWORDS: *layer-by-layer deposition, organic crystals, organic field-effect transistor*

INTRODUCTION

Understanding the relationship between the morphological structures of a semiconducting organic crystal and the electrical properties of such crystals is important for improving the performances of organic electronic devices,[1−3] such as organic thin film transistors (OTFTs).[4−7] The morphology of a thin film organic crystal is significantly influenced by the crystal growth mechanism. Two-dimensional (2D) layer-by-layer crystal growth is more desirable than three-dimensional (3D) island growth for achieving high charge carrier mobilities in semiconducting organic crystals.[4,8,9] The coarse grain boundaries that form through the coalescence of three-dimensionally growing grains act as trap sites.

It is difficult to grow organic crystals on a substrate surface via 2D layer-by-layer growth with a precision that rivals the precision obtained by vacuum-depositing inorganic materials. Films prepared from organic molecules suffer from a greater surface roughness compared to films composed of atoms because organic molecules tend to have a low symmetry that can produce strain in their films grown on the substrates.[10,11] Charge transport paths over defective grain boundaries in an organic crystal may be prepared with good connectivity by depositing the crystalline films such that the film thickness is several tens of monolayers.[12−14] To this end, it is important to create an effective method for growing organic crystals in a layer-by-layer mode and to demonstrate reasonable electrical performances, even at a thickness of only a few molecular layers.

Self-assembled monolayer (SAM)-based methods of optimizing an organic−substrate interface[15−17] show promise for the growth of high-quality crystalline active layers; however, SAMs can only influence the interactions between the substrate and the first crystalline layer.[18,19] They cannot prevent secondary nucleation over the surface of a preformed crystalline layer. Therefore, in addition to modifying the substrate surfaces, semiconducting molecules must be designed to have an inherent tendency to assemble through a 2D layer-by-layer crystal growth mechanism.

Most semiconducting organic molecules have π-conjugated aromatic backbone along their long molecular axis. They crystallize more or less with a vertical orientation on the substrate surface such that the charge carriers transport by hopping over the laterally packed molecules. The first crystalline layer in these conjugated molecules grows laterally in a 2D growth mode during the initial period of deposition. The islands then grow on top of the monolayer via secondary nucleation before the substrate surface is fully covered with the first monolayer.[11,20] A key difference between the initial and later stages of organic crystal growth is that the surface on which the molecules are deposited transitions from the substrate to the organic crystal itself. The substrate and crystal usually differ in their surface chemistries. The surfaces of growing organic crystals are usually more hydrophobic and have a lower surface energy than an inorganic oxide substrate surface. To enhance the 2D growth in the upper layers, it is

Received: May 29, 2013
Accepted: July 16, 2013
Published: July 16, 2013

   dx.doi.org/10.1021/am402066t | ACS Appl. Mater. Interfaces 2013, 5, 6837−6842

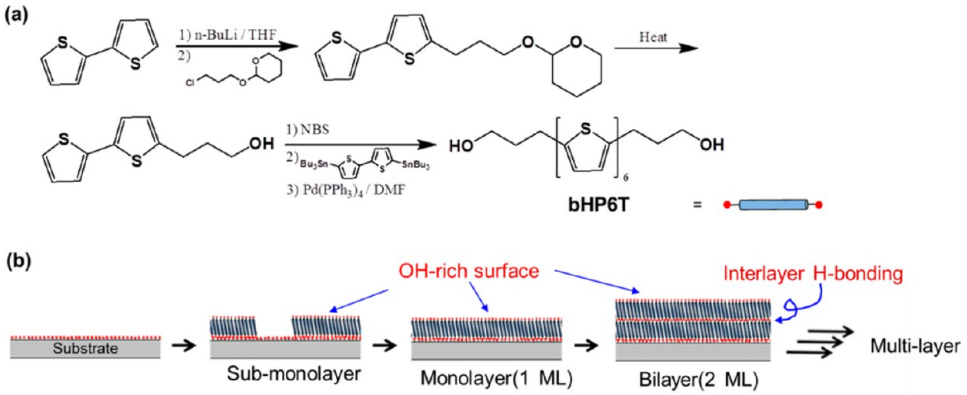

Figure 1. (a) Synthesis of bHP6T and (b) schematic representation of the H-bonding-facilitated layer-by-layer growth of bHP6T thin film crystals.

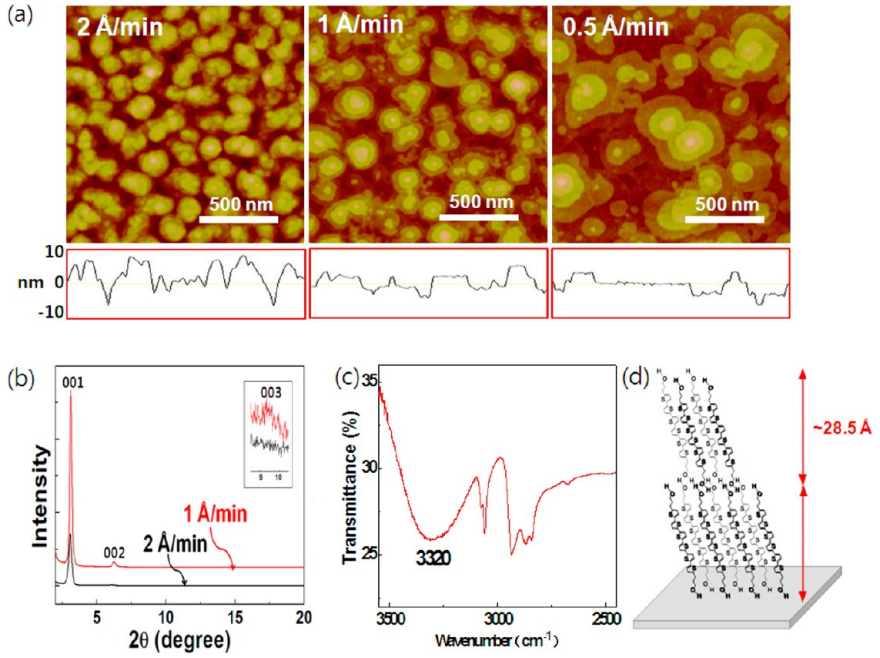

Figure 2. Characteristics of the 50 nm thick bHP6T crystal films: (a) Height contrast AFM images grown at deposition rates of 2, 1, and 0.5 Å/min, respectively; (b) XRD curves of the films grown at 1 and 2 Å/min, respectively; (c) FT-IR spectrum showing the OH stretching band, indicating the presence of H-bonded hydroxyl groups; and (d) a schematic illustration of the layered bHP6T packing structure.

essential for the molecules to have a structure that facilitates lateral molecular packing and interlayer interaction.

Here we demonstrate that the symmetric attachment of hydroxyalkyl groups onto semiconducting organic molecules provides an efficient synthetic approach to facilitating 2D layer-by-layer growth in organic crystals. We synthesized bis(3-hydroxypropyl)-sexithiophene (bHP6T) consisting of a conjugated sexithiophene(α6T) backbone and 3-hydroxypropyl groups (Figure 1). Once a crystalline monolayer of the molecules forms on the surface, the hydroxyalkyl groups are configured at the top surface, yielding a surface with H-bonding capability. 2D growth of an overlayer may be facilitated by interlayer H-bonding and lateral intermolecular H-bonding interaction. The generation of hydroxyl-rich surfaces is then repeated layer-by-layer to provide conditions that are suitable for promoting the 2D growth of an overlayer.

RESULTS AND DISCUSSION

bHP6T molecules were thermally evaporated onto the substrate at 30 °C. The bHP6T films were optimized by varying the deposition rate from 0.1 to 2 Å/min. The evaporation of bHP6T molecules at a deposition rate exceeding 2 Å/min yielded granules that grew irregularly (Figure 2a). Terraced crystals developed in all samples, and larger grains were produced at lower deposition rates.

X-ray diffraction (XRD) studies of the bHP6T films exhibited (001), (002), and (003) scattering peaks corresponding to a multilayered structure with a *d*-spacing of 2.85 nm (Figure 2b). Stronger scattering peaks appeared for film grown at lower deposition rates, consistent with the AFM images. Grazing incidence small-angle X-ray scattering (GI-SAXS) also revealed clearly the multilayered structure (see Figure S3 in the Supporting Information). The FT-IR spectra of the crystals exhibited a strong OH stretching band near 3320 cm^{-1}, indicating that most hydroxyl groups in the crystals had formed hydrogen bonds.[21] The observed layer periodicity was smaller than the length (3.16 nm) of a stretched bHP6T molecule, suggesting a tilt at the junction between the aromatic backbone and the hydroxypropyl groups, as illustrated in Figure 2d and similar to that reported previously for dialkyl 6T.[22,23]

dx.doi.org/10.1021/am402066t | ACS Appl. Mater. Interfaces 2013, 5, 6837−6842

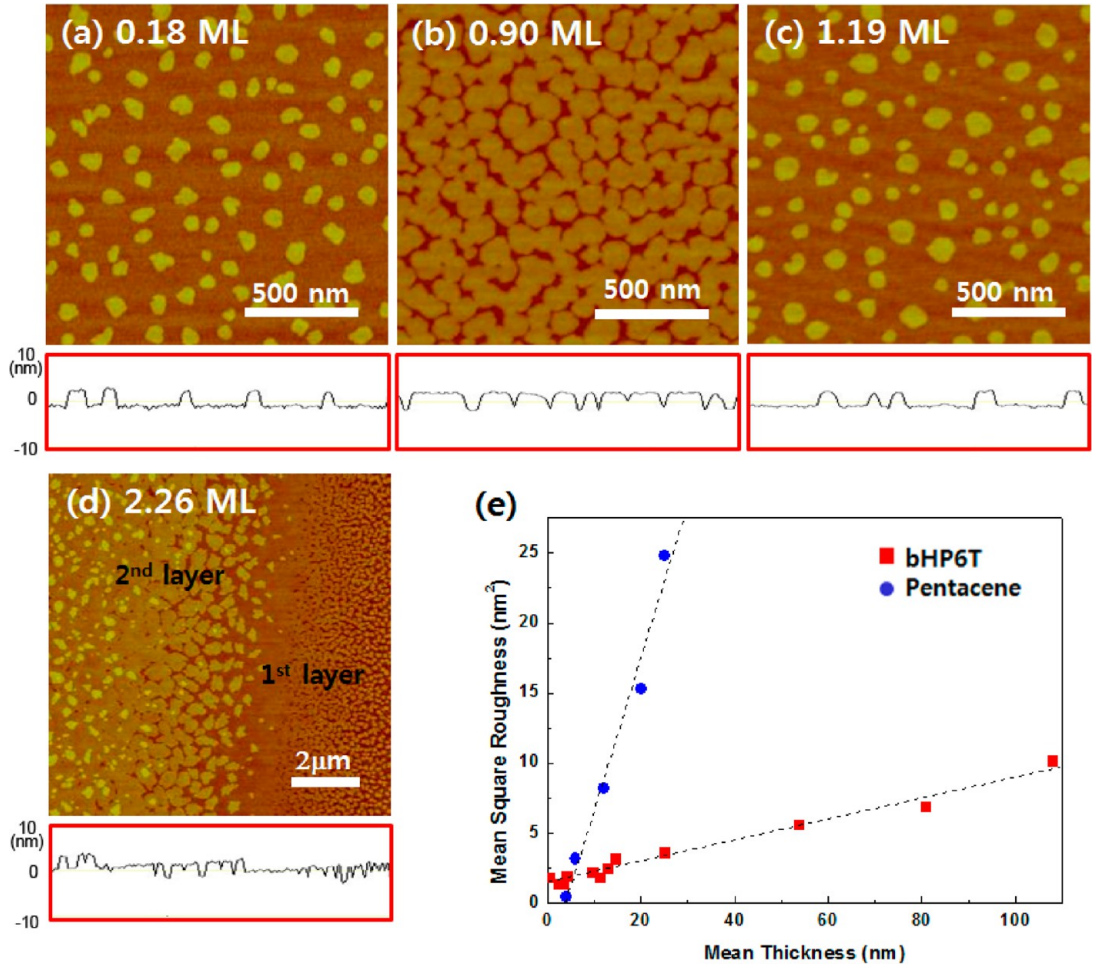

Figure 3. Layer-by-layer growth of bHP6T crystals deposited onto a silica surface at a rate of 1 Å/min at room temperature. (a–c) Height contrast tapping mode AFM images of the films prepared with thickness values of 0.18, 0.90, and 1.19, respectively. The 1 ML film fully covered the substrate with a single layer; (d) The AFM image of the terraced edge of the vacuum-deposited 2.26 ML film; and (e) graph of the mean square roughness versus the mean thickness of the vacuum-deposited bHP6T and pentacene crystals. The data for the pentacene films were obtained from the literature.[26].

The AFM images of the 50 nm thick films shown in Figure 2 exhibited relatively low surface roughness values. The films grown at low deposition rates showed a roughness corresponding to only a few ML in thickness, suggesting that the film was grown by the layer-by-layer mechanism. The layer-by-layer growth of bHP6T films was clearly evident in a series of AFM images that showed the formation of submonolayers and multilayers, as shown in Figure 3. The surface coverage and nucleation density[17,24] of the bHP6T crystals on the top layer were estimated from the AFM images collected from films of different thickness (see Figure S4 in the Supporting Information), as summarized in Table S1 in the Supporting Information. The first layer continued to grow laterally until the surface coverage reached 96%. The nuclei of the second layer began to appear after the surface was nearly fully covered with the crystalline film. Remarkably, the growth pattern at 0.18 ML thickness was nearly identical to that at 1.19 ML thickness, indicating that the nucleation density and grain size of the bHP6T submonolayer on the silica substrate were almost identical to the values obtained for the second monolayer at a similar surface coverage (θ).

The growth behavior of the bHP6T crystals was distinct from the layer-plus-island growth mode generally observed for most organic crystals grown on inorganic substrates at low temperatures, in which the second layer began to appear near a surface coverage of 80% at most,[20,25] and then the organic crystals grew in the 3D island-type growth mode.

A clear distinction between the layer-by-layer-grown bHP6T crystals and one of other organic crystals grown via the 3D island growth mode is evident in Figure 3e, which shows the mean square surface roughness plotted against the mean thickness of the vacuum-deposited bHP6T and pentacene crystals. The roughness data were obtained from the AFM images in Figure S5 in the Supporting Information. The thicknesses of the films were measured by imaging the edge region of the films, as shown in Figure 3d. The thicknesses of films thicker than 3 ML were measured using AFM after scratching the films with a razor blade. The dependence of the mean square surface roughness of the bHP6T films on the film thickness was compared with the dependence reported for pentacene[26] and that obtained for 6T (see Figure S6 in the Supporting Information) grown at a relatively low deposition rate. The roughness increase per unit thickness in the bHP6T films was only about 10 and 25% the roughness increase observed in the pentacene and 6T films, respectively. The transition from layer to island growth mode is evident for both 6T and pentacene.

dx.doi.org/10.1021/am402066t | ACS Appl. Mater. Interfaces 2013, 5, 6837–6842

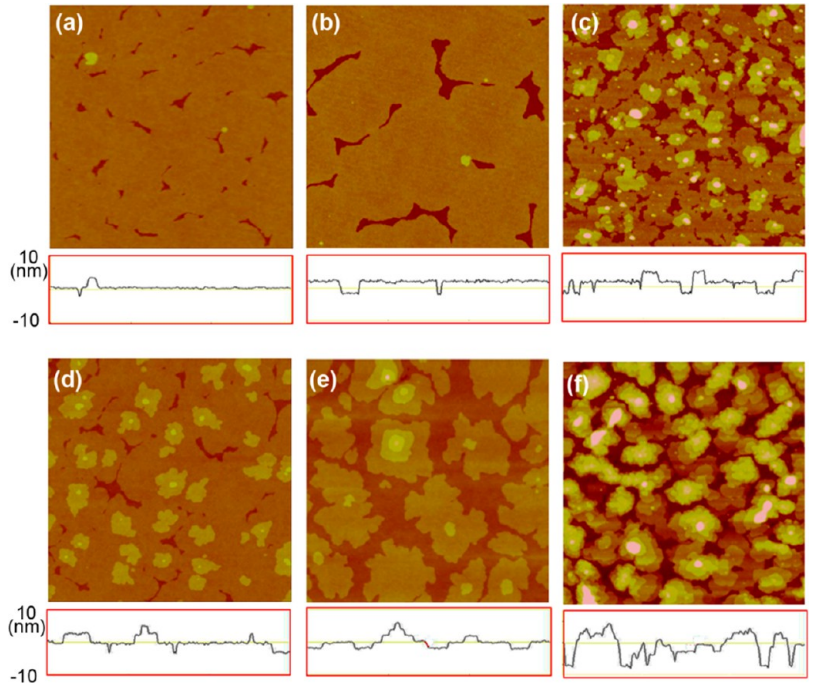

Figure 4. Height contrast AFM images of the bHP6T crystals grown on (a, d) silica, (b, e) HMDS SAM, and (c, f) ODTS SAM surfaces. The deposition rate was 0.1 Å/min; film thickness (a–c) 3 and (d–f) 9 nm. The image size was 3 × 3 μm^2.

It is noteworthy that the grains of pentacene and 6T molecules on top of the first layer exhibited more dendritic pattern and were larger than those on the substrate surface, indicating that the surface diffusion contributed more to the overlayer crystal growth in 6T and pentacene as compared with that in bHP6T. This may be accounted for by that the interaction between the 6T or pentacene molecules and their monolayer surface is relatively weaker than that between bHP6T and its monolayer.

The effects of the substrate surface energy on the bHP6T film growth mechanism in the first few layers were clearly evident in the AFM images (Figure 4) of the bHP6T films deposited on bare silica, hexamethyldisilazane (HMDS) SAM, or octadecyltrichlorosilane (ODTS) SAM surfaces at the same temperature and deposition rate. The water contact angles of these surfaces were measured to be 30, 75, and 105°, respectively. The water contact angles of the bHP6T films were 80°. The AFM images showed that the crystals grown on the ODTS SAM were distinct from the 2D layer-by-layer crystals grown on the silica or HMDS SAM surfaces. Many secondary nuclei formed before the ODTS SAM surface had been fully covered with a crystalline layer.

The ability to grow crystals in a nearly 2D growth mode both in the first layer and its overlayers enabled the fabrication of an active organic layer only a few molecules thick. We deposited films using a stepwise deposition rate: a rate of 0.1 Å/min was used to deposit films thinner than 3 ML (9 nm, Figure 4), and then a rate of 1 Å/min was used to deposit thicker films. Interestingly, the morphologies of the films grown on different surfaces were similar at a thickness of 25 nm (see Figure S8 in the Supporting Information).

We examined the performances of OFET devices prepared with bHP6T films of various thicknesses in a top-contact configuration (see Figures S6 and S7 and Table S2 in the Supporting Information). The devices with 1–2 ML layer thicknesses exhibited charge carrier mobility below 1 × 10^{-4} $cm^2/(V\ s)$ and an on/off ratio of 1 × 10^3. These low performance parameters can be attributed to the metal penetration effects in the very thin devices.[27] The bHP6T films thicker than 9 nm (3 ML) yielded mobilities of 0.018–0.070 $cm^2/(V\ s)$ and on–off ratios of 1 × 10^4 to 1 × 10^6. These results exceeded the values reported for other sexithiophene derivatives with much thicker active layers.[28,29] It is particularly noteworthy that only the 9 nm thick films exhibited a reasonable performance. Our results contrasted with the FET performances (1 × 10^{-3} to 1 × 10^{-4} cm^2/V) reported previously for hydroxyalkyl oligothiophenes.[30] The low performance of those films most likely resulted from the use of deposition rates that were not optimal for promoting layer-by-layer growth.

Although the silanol groups in the interfacial regions can act as trap sites and hinder charge transport,[31−33] it is unclear whether the alkyl alcohol group in the bHP6T crystals cause the same effects on the electrical performance. Interestingly, our devices were resistant to degradation upon exposure to atmospheric conditions. We monitored the performances of the bHP6T TFTs during exposure to ambient air over 30 days. The electrical mobilities and on/off ratios of the bHP6T devices decreased to 0.015–0.046 $cm^2/(V\ s)$ and 1 × 10^4 to 1 × 10^5, respectively (see Table S2 in the Supporting Information). These values remained nearly constant over two months. It should be noted that the extent of degradation in our ultrathin devices was smaller than that in any other organic device reported previously.[34,35] The hydroxyl groups may have efficiently segregated from the charge-transporting 6T lamellar crystal multilayers, thereby avoiding interfering with charge transport. We postulated that the 2D crystal growth mode generated fewer grain boundaries within the crystals, which prevented moisture from readily forming penetration paths. Improved air stability in hydrogen-bonded organic semiconductors has been reported recently by others.[36]

CONCLUSIONS

In summary, we demonstrated that oligomeric semiconducting molecules with α,ω-bis(hydroxyalkyl) groups may be vacuum-deposited to form ultrathin crystalline films via a nearly perfect layer-by-layer growth mode to utilize the hydrogen bonding capability of the molecule. The electrical performances of crystalline bHP6T films only a few monolayers thick were comparable to the performances of other known sexithiophene derivatives. Efficient multilayered packing during the enhanced 2D growth mode appeared to offer a more stable performance against atmospheric degradation.

EXPERIMENTAL SECTION

Materials. All solvents and reagents were obtained from commercial sources and used without further purification, unless otherwise noted. THF was distilled under a nitrogen atmosphere from Na/benzophenone prior to use. 2,2′-Bithiophene (2T; 97%, Aldrich) was purified by sublimation. 2-(3-Chloropropoxy) tetrahydro-2H-pyran (97%, Aldrich) and tributyltin chloride (96%, Aldrich) were distilled under reduced pressure. Silica (230−400 mesh) and TLC were purchased from Merck. 5-(3-Tetrahydropyran-2-yloxypropyl)-2,2′-bithiophene and 5-(3-hydroxypropyl)-2,2′ bithiophene were synthesized by known method[37] as an oil in 42% and 98% yield, which was used as the starting compound for bHP6T molecules. 5,5′-Bis(tri-n-butylstannyl)-2,2′-bithiophene was synthesized by following known method[38] as a liquid in 88% yield.

Synthesis of bHP6T. 5-(3-Hydroxypropyl)-2,2′ bithiophene (2.7g, 12.0 mmol) was dissolved in 50 mL of THF. To the solution was added N-bromosuccinimide (NBS, 2.16 g, 12.0 mmol) at −20 °C for 1h. The mixture was slowly warmed up to room temperature and stirred for overnight. The reaction was terminated by addition of 10% solution of KOH. Diethyl ether was added, and the organic layer was concentrated and dried over anhydrous $MaSO_4$. The crude product was purified by chromatography eluting with ethyl acetate/petroleum ether. The yield of 5-bromo-5′-hydroxypropyl-2,2′-bithiophene was 30.8% based on consumed starting materials.

To a stirred solution of 5-bromo-5′-hydroxypropyl-2,2′-bithiophene (1.09 g, 3.13 mmol) in DMF (20 mL) were added a solution of 5,5′-Bis(tri-n-butylstannyl)-2,2′-bithiophene (1.17 g, 1.6 mmol) in anhydrous DMF (20 mL) and a catalytic amount of $Pd(PPh_3)_4$, successively. The solution was stirred near 100 °C for 8 h. After the mixture was cooled and the red solid product was filtered and washed sequentially with ether, dichloromethane, and tetrahydrofuran. Further purification was carried out by Soxhlet extraction with toluene and THF. MALDI-TOF MS with 2,5-dihydroxy benzoic acid (DHB) as matrix: m/z 610.17, calcd 610.03.

Characterization. Materials were characterized using ^1H NMR spectroscopy (JEOL JNM-LA 400WBFT-NMR) in deuterated chloroform ($CDCl_3$, min. 99.96 atom %D). The FT-IR spectra were recorded on a Perkin-Elmer FT-IR spectrometer, Spectrum 2000. Differential scanning calorimetry (DSC) was carried out using a TA Instruments 2010 series instrument at a heating rate of 10 °C/min under a nitrogen atmosphere. Mass spectra were obtained using matrix-assisted laser desorption ionization time-of-flight mass spectrometry (MALDI TOF-MS, Applied Biosystems Voyager-DE STR in ion mode) using 2,5-dihydroxy benzoic acid (DHB) as the matrix. Atomic force microscopy (AFM) stabilized by anti-vibration specialists (HALCYONICS) was conducted in the tapping mode using a Digital Instruments Multimode AFM (Veeco), controlled by a Nanoscope IIIa scanning probe microscope controller. Phosphorus (n) doped Si with spring constant of 20−80 N/m (Model: RTESP, Veeco) and cantilever of 11 −135 μm long was used for TM-AFM. X-ray diffraction (XRD) was performed at room temperature using Rint 2200 V, RIGAKU Co., Ltd., which was operated at 40 kV and 100 mA with λ = 1.542 Å. Small/wide-angle X-ray scattering (S/WAXS) measurement was performed using equipment (SAXSess, Anton Paar) connected to an X-ray generator (PW 3830, 4 kW, PANalytical) operated at 40 kV and 40 mA with a sealed tube Cu anode (λ = 1.542 Å). Sample for S/WAXS measurement was prepared by pelletized and then placed in the sample holder. Grazing-incidence small-angle X-ray scattering (GI-SAXS) measurement was carried out with SAXSess (Anton Paar) connected to an X-ray generator (ID3003, SEIFERT Analytical X-ray) operated at 40 kV and 50 mA. The SAXSess camera was mounted on the point-focus outlet of a sealed tube Cu anode (λ = 1.542 Å). For GI-SAXS measurement, thick film (thickness = 80 nm) was prepared by deposition of bHP6T on silica surface at a deposition rate of 2 Å/min at room temperature. Incident angle was set to 0.2°, controlled by Vario Stage Control Unit. The 2D scattering patterns were recorded by an imaging plate detector and were read out by OptiQuantTM image analysis software (Perkin-Elmer). They were converted to 1D profile using SAXS-quantTM software (Anton Paar). The scattering data were represented in the scattering vector q, defined by $q = (4\pi/\lambda)\sin(\theta)$. The d-spacing was calculated by $d = 2\pi/q$.

SAM Preparation. n-Type doped (100) Si wafers with 3000 Å thick SiO_2 were sonication-treated successively in acetone, isopropanol, and deionized water for over 5 min twice. After DI-water rinsing, the substrates were dried by N_2 stream and then placed in the oven at 100 °C for 30 min. The substrates were then treated by oxygen plasma (using Harrick Plasma cleaner DDC-32G) for 2 min. HMDS surfaces were prepared by spin-coating using 20% dilute HMDS solution in propylene glycol monomethyl ether acetate (PGMEA) at the spin speed of 4000 rpm for 35 s. After soft bake at 100 °C for 30 min, HMDS surfaces were sonication-treated successively in isopropanol and deionized water for over 5 min twice and dried at 100 °C for 30 min. ODTS surfaces were prepared by immersion-coating in ∼1% anhydrous toluene solution for overnight. ODTS surfaces were sonication-treated successively in acetone, isopropanol, and deionized (DI) water for over 5 min twice and dried at 100 °C for 30 min.

OTFT Device Fabrication and Characterization. We used highly n-type doped (100) Si wafers with thermally grown SiO_2 that was 3000 Å thick and served as the gate dielectric. bHP6T was deposited on the substrates using thermally evaporation method under high vacuum conditions (about 1 × 10^{-7} Torr) at room temperature. The deposition rates and film thickness were measured using a quartz-crystal thin-film thickness monitor of the thermal evaporator. After bHP6T deposition, gold source and drain electrodes were thermally evaporated onto the organic film through a shadow mask at a rate of about 0.3 Å/s. The channel length (L) and channel width (W) on the mask were 100 μm and 5 mm, respectively. The electrical properties of these devices were measured using a KEITHLEY 2400 semiconductor characterization system in a glovebox.

■ ASSOCIATED CONTENT

Supporting Information

Characteristics of bHP6T molecules, AFM images of the bHP6T and α-sexithiophene (6T) crystals grown to various thicknesses; S/WAXS and GI-SAXS spectra of the bHP6T powder and films; output and transfer curves of the bHP6T-based OTFTs; and the TFT performance data before and after air exposure. This material is available free of charge via the Internet at http://pubs.acs.org.

■ AUTHOR INFORMATION

Corresponding Author

*E-mail: jiwoong@gist.ac.kr.

Notes

The authors declare no competing financial interest.

■ ACKNOWLEDGMENTS

This research was supported by the Basic Science Research Program (NRF-2010-0026421) through the National Research Foundation of Korea (NRF), funded by the Ministry of Education, Science, and Technology of Korea, and by the Program for Integrated Molecular Systems (PIMS) at GIST.

■ REFERENCES

(1) Tsao, H. N.; Mullen, K. *Chem. Soc. Rev.* **2010**, *39*, 2372−2386.
(2) Muccini, M.; Murgia, M.; Biscarini, F. *Adv. Mater.* **2001**, *13*, 355−358.
(3) DeLongchamp, D. M.; Kline, R. J.; Jung, Y.; Germack, D. S.; Lin, E. K.; Moad, A. J.; Richter, L. J.; Toney, M. F.; Heeney, M.; McCulloch, I. *ACS Nano* **2009**, *3*, 780−787.
(4) Shao, W.; Dong, H.; Jiang, L.; Hu, W. *Chem. Sci.* **2011**, 2.
(5) Dinelli, F.; Murgia, M.; Levy, P.; Cavallini, M.; Biscarini, F.; de Leeuw, D. M. *Phys. Rev. Lett.* **2004**, *92*, 116802.
(6) Di, C.-a.; Liu, Y.; Yu, G.; Zhu, D. *Acc. Chem. Res.* **2009**, *42*, 1573−1583.
(7) Mas-Torrent, M.; Rovira, C. *Chem. Rev.* **2011**, *111*, 4833−4856.
(8) Sassella, A.; Campione, M.; Papagni, A.; Goletti, C.; Bussetti, G.; Chiaradia, P.; Marcon, V.; Raos, G. *Chem. Phys.* **2006**, *325*, 193−206.
(9) Verlaak, S.; Steudel, S.; Heremans, P.; Janssen, D.; Deleuze, M. S. *Phys. Rev. B* **2003**, *68*, 1954091−19540911.
(10) Hooks, D. E.; Fritz, T.; Ward, M. D. *Adv. Mater.* **2001**, *13*, 227−241.
(11) Ward, M. D. *Chem. Rev.* **2001**, *101*, 1697−1726.
(12) Biscarini, F.; Zamboni, R.; Samorí, P.; Ostoja, P.; Taliani, C. *Phys. Rev. B* **1995**, *52*, 14868−14877.
(13) Gundlach, D. J.; Lin, Y. Y.; Jackson, T. N.; Nelson, S. F.; Schlom, D. G. *IEEE Electron Device Lett.* **1997**, *18*, 87−89.
(14) Lovinger, A. J.; Davis, D. D.; Dodabalapur, A.; Katz, H. E.; Torsi, L. *Macromolecules* **1996**, *29*, 4952−4957.
(15) Hill, I. G.; Weinert, C. M.; Kreplak, L.; Zyl, B. P. *Appl. Phys. A: Mater. Sci. Process.* **2009**, *95*, 81−87.
(16) Islam, M. M.; Pola, S.; Tao, Y.-T. *ACS Appl. Mater. Interfaces* **2011**, *3*, 2136−2141.
(17) Jeong, S.-M.; Park, J.-W. *J. Am. Chem. Soc.* **2008**, *130*, 3497−3501.
(18) Hiremath, R.; Varney, S. I.; Swift, J. A. *Chem. Mater.* **2004**, *16*, 4948−4954.
(19) Yang, H. C.; Shin, T. J.; Ling, M. M.; Cho, K.; Ryu, C. Y.; Bao, Z. N. *J. Am. Chem. Soc.* **2005**, *127*, 11542−11543.
(20) Meyer zu Heringdorf, F. J.; Reuter, M. C.; Tromp, R. M. *Nature* **2001**, *412*, 517−520.
(21) Belkov, M. V.; Ksendzov, G. A.; Polozov, G. I.; Skornyakov, I. V.; Sorokin, V. L.; Tolstorozhev, G. B.; Shadyro, O. I. *J. Appl. Spectrosc.* **2010**, *77*, 496−501.
(22) Facchetti, A.; Yoon, M.-H.; Stern, C. L.; Hutchison, G. R.; Ratner, M. A.; Marks, T. J. *J. Am. Chem. Soc.* **2004**, *126*, 13480−13501.
(23) Fichou, D. *J. Mater. Chem.* **2000**, *10*, 571−588.
(24) Ruiz, R.; Choudhary, D.; Nickel, B.; Toccoli, T.; Chang, K. C.; Mayer, A. C.; Clancy, P.; Blakely, J. M.; Headrick, R. L.; Iannotta, S.; Malliaras, G. G. *Chem. Mater.* **2004**, *16*, 4497−4508.
(25) Yang, J.; Wang, T.; Wang, H.; Zhu, F.; Li, G.; Yan, D. *J. Phys. Chem. B* **2008**, *112*, 7821−7825.
(26) Wang, S. D.; Dong, X.; Lee, C. S.; Lee, S. T. *J. Phys. Chem. B* **2005**, *109*, 9892−9896.
(27) Braga, D.; Horowitz, G. *Adv. Mater.* **2009**, *21*, 1473−1486.
(28) Dell'Aquila, A.; Mastrorilli, P.; Nobile, C. F.; Romanazzi, G.; Suranna, G. P.; Torsi, L.; Tanese, M. C.; Acierno, D.; Amendola, E.; Morales, P. *J. Mater. Chem.* **2006**, *16*, 1183−1191.
(29) Murphy, A. R.; Fréchet, J. M. J. *Chem. Rev.* **2007**, *107*, 1066−1096.
(30) Katz, H. E.; Johnson, J.; Lovinger, A. J.; Li, W. *J. Am. Chem. Soc.* **2000**, *122*, 7787−7792.
(31) Chua, L.-L.; Zaumseil, J.; Chang, J.-F.; Ou, E. C. W.; Ho, P. K. H.; Sirringhaus, H.; Friend, R. H. *Nature* **2005**, *434*, 194−199.
(32) Gi Choi, C.; Bae, B.-S. *Electrochem. Solid-State Lett.* **2007**, *10*, H347−H350.
(33) Yoon, M. H.; Kim, C.; Facchetti, A.; Marks, T. J. *J. Am. Chem. Soc.* **2006**, *128*, 12851−12869.
(34) Daisuke, K.; Tokiyoshi, U.; Shizuo, T. *Appl. Phys. Lett.* **2008**, *92*, 093309.
(35) Jan Hendrik, S. *Appl. Phys. Lett.* **2001**, *79*, 4163−4164.
(36) Głowacki, E. D.; Irimia-Vladu, M.; Kaltenbrunner, M.; Gsiorowski, J.; White, M. S.; Monkowius, U.; Romanazzi, G.; Suranna, G. P.; Mastrorilli, P.; Sekitani, T.; Bauer, S.; Someya, T.; Torsi, L.; Sariciftci, N. S. *Adv. Mater.* **2013**, *25*, 1563−1569.
(37) Katz, H. E.; Laquindanum, J. G.; Lovinger, A. J. *Chem. Mater.* **1998**, *10*, 633−638.
(38) Wei, Y.; Yang, Y.; Yeh, J.-M. *Chem. Mater.* **1996**, *8*, 2659−2666.